Control of Carboxylic Acid and Ester Groups on Chromium (VI) Binding to Functionalized Silica/Water Interfaces Studied by Second Harmonic Generation

Hind A. Al-Abadleh, Amanda L. Mifflin, Paul A. Bertin, SonBinh T. Nguyen, and Franz M. Geiger*

Department of Chemistry and the Center for Nanofabrication and Molecular Self-Assembly, Northwestern University, 2145 Sheridan Road, Evanston, Illinois 60208

Received: February 14, 2005; In Final Form: March 9, 2005

Resonantly enhanced surface second harmonic generation (SHG) measurements carried out at pH 7 and room temperature were performed to study how surface-bound carboxylic acid and methyl ester functional groups control the interaction of chromate ions with fused silica/water interfaces. These functional groups were chosen because of their high abundance in humic and fulvic acids and related biopolymers commonly found in soils. They were anchored to the silica surface using organosilane chemistry to avoid competing complexation processes in the aqueous solution as well as competitive adsorption of the organic compounds and chromate. The SHG experiments were carried out at room temperature and pH 7 while using environmentally representative chromate concentrations ranging from 1×10^{-6} to 2×10^{-4} M. Chromate is found to bind to the acid- and ester-functionalized silica/water interfaces in a reversible fashion. In contrast to the plain silica/water interface, chromate binding studies performed on the functionalized silica/water interfaces show S-shaped adsorption isotherms that can be modeled using the Frumkin−Fowler−Guggenheim (FFG) model. This model predicts a coverage-dependent binding constant of $K_{ads} \times \exp(g\theta)$. Values for g are found to be 3.2(2), 2.1(2), and 1.3(2) for the carboxylic acid-, the ester-, and the nonfunctionalized silica/water interfaces, respectively, and are consistent with stabilizing lateral adsorbate−adsorbate interactions among the Cr(VI) species adsorbed to the functionalized surfaces. The FFG model allows for the parametrization of the solid−liquid partition coefficient and chromate retardation factors in silica-rich soil particles whose surfaces contain organic adlayers rich in carboxylic acid and methyl ester groups. The straightforward model presented here predicts that chromate retardation increases by up to 200% when carboxylic acid functional groups are present at the silica/water interface. Increases up to 50% are predicted for methyl ester-containing organic adlayers, and the retardation factor remains effectively near unity for the plain silica/water interface (no siloxanes present).

I. Introduction

Biosurfactants and biopolymers are important in the chemistry of environmental interfaces because they can change the surface properties of mineral oxide particles in the environment.[1−5] Biosurfactants originating from soil microbial excretions and cell fragments often contain surface-active organic functional groups that can bind to mineral surfaces. Likewise, biopolymers commonly found in natural organic matter (NOM) or soil organic matter (SOM) include humic and fulvic acids,[6] which have complex structures consisting of polar di- or trihydroxy-phenol groups, quinone moieties and α-hydroxy-carboxylic acid and ester groups that can interact with mineral oxides and change their surface properties. As such, organic adlayers at mineral oxide/water interfaces can control the chemical composition of aqueous phase pollutants by binding aqueous phase trace metals in subsurface environments.[1−4,7,8] A specific example of such a metal is chromium. The carcinogenicity, toxicity, and the widespread contamination of chromium in populated areas[9−23] have earned this transition metal a place on the EPA list of priority pollutants. The highest allowable limit for total chromium in groundwater in the U.S. is 2×10^{-6} M,[24] whereas many polluted sites exhibit chromium concentrations that are several orders of magnitude higher.[10]

Under oxidizing conditions and neutral pH, chromate, CrO_4^{2-}, is the dominant stable form of chromium in aqueous solutions.[25] In general, dissolved iron(II) and/or minerals that contain redox-active metal species can lower the concentration of chromate in the aqueous phase by reducing it to Cr(III), the much less mobile, second most stable oxidation state of chromium in the environment.[9] However, Fe(II) concentration levels in many soil environments may not always be high enough for efficient chromate reduction.[26] In these cases, NOM can act either as an important chelator for aqueous-phase Cr(VI)[27−31] or aid in the reduction of Cr(VI) when redox-active metal species are present under low pH conditions.[32−37]

In solution, possible mechanisms for chromate reduction by NOM include electrostatic interactions[38] that emphasize chromate chelation by functional groups common to NOM.[32,39] Wittbrodt and Palmer studied the interaction of chromate ions with soil humic substances and determined that the rates of chromate reduction by soil fulvic acid increase markedly with decreasing pH.[33] In contrast, Deng and Stone showed that, at pH 4.7, the bulk aqueous phase redox chemistry between chromate and model α-hydroxy-carboxylic acids and their esters is negligible for chromate concentrations of 2×10^{-5} M and concentrations for the organic compounds that are 10 times higher.[40] In general, chromate reduction rates by organic compounds with oxygen-containing functional groups have half-lives on the order of months to years at pH 7 if redox-active

* To whom correspondence should be addressed. E-mail: geigerf@chem.northwestern.edu.

10.1021/jp050782o CCC: $30.25
Published on Web 04/07/2005

metal species (in the aqueous or solid state) are absent.[41] The extensive literature[42−45] on the acid-catalyzed oxidation of organic compounds by Cr(VI) may be used as a guideline for studying NOM-mediated Cr(VI) reduction processes under acidic conditions.

The focus of this work is to track the interaction of chromate with different aqueous/solid interfaces that are important in aquatic geochemistry but do not possess redox properties. By working under neutral pH conditions and in the absence of redox-active metal ions, we can focus on specifically studying the interaction of chromate with surface-bound organic functional groups. To investigate how surface-bound carboxylic acid and ester functional groups control chromate binding to mineral oxide/water interfaces, a reductionist approach is chosen here. Our strategy is to turn off chelating interactions between dissolved chromate and the dissolved organic species in the aqueous phase by decorating the solid substrate surfaces with organosilanes that are chemically bound to the substrate and that contain the specific organic functional groups under investigation. This strategy also circumvents issues arising from the coadsorption of chromate and the organic species. Since silica is a common mineral found in many soils, we patterned silica surfaces with carboxylic acid- and methyl ester-functionalized silanes, which is a straightforward task using siloxane attachment chemistry.[46,47] The resulting platform affords a versatile model system for studying the interaction of aqueous phase pollutants with a wide variety of organic adlayers on mineral surfaces. In addition, our strategy is ideal for generating organic adlayers that effectively simulate biosurfactants and related surface-active species with high control over the chemistry, structure, and order of the surface-bound environmentally relevant molecules, while reactivity issues commonly encountered in thiol/gold systems are avoided. The organic adlayers used in this work have been characterized using the nonlinear optical spectroscopy techniques, vibrational sum frequency generation (SFG),[48] and second harmonic generation (SHG).[49] In this work, surface-bound Cr(VI) is monitored by resonantly enhanced SHG. As we highlighted in our earlier work,[50,51] SHG affords surface specificity and provides spectroscopic, thermodynamic, and kinetic information under environmentally relevant temperatures, pH conditions, and chromate concentrations. Recently, we showed that the interaction of chromate with the silica/water interface is fully reversible,[51] which is consistent with the reported high mobility of Cr(VI) in most soil environments.[9,35,52−57] Free energies of adsorption are consistent with hydrogen bonding interactions, and binding constants obtained from both thermodynamic and kinetic studies of chromate adsorption to silica/water interfaces were used in a simple chemical transport model.[50] CrO_4^{2-} protonation at low pH forming $HCrO_4^-$ may be important for Cr(VI) adsorption as well.[50,51]

By comparing surface-specific data derived from the functionalized silica/water interfaces with data obtained from the plain silica/water interface (no organic adlayers present), one can assess how various environmentally important organic functional groups at mineral oxide/water interfaces control toxic metal binding. This information is crucial for enhancing the accuracy of pollutant transport models through an improved understanding of chromate retardation, i.e., extent of transport, in soils.

II. Experimental Section

Pump−Flow Setup and Laser System. The binding behavior of chromate to the siloxane-functionalized silica/water interfaces was studied in situ and in real time using resonantly enhanced surface second harmonic generation (SHG). Simultaneously with the SHG experiments, the bulk chromate concentration was recorded using UV−vis spectroscopy (Ocean Optics, 185−850 nm). Experiments were conducted using the dual pump−flow and laser systems described in detail previously.[50,51] Briefly, after deposition of the siloxane adlayers (vide infra), the flat side of the 1 in.-diameter fused quartz hemispherical lens (ISP Optics) was clamped leak-tight to a custom-built Teflon liquid flow cell through a Viton O-ring. The flow cell was connected to the chromium solution (K_2CrO_4, ICN Biomedicals), water (Millipore, 18 MΩ), and waste reservoirs through Tygon tubing and Teflon fittings (Swagelok). The aqueous phase was pumped across the interface using flow-controlled peristaltic pumps (Fisher). A flow meter (Fisher) was placed after the mixing point of the potassium chromate solution with water and before the flow cell for flow rate measurements. The pH of the potassium chromate solution and water was held at pH 7 using standard solutions of NaOH and HCl (Fisher).

The experiments were run under controlled-flow conditions. Initially, water was pumped at a rate equivalent to about 0.52 mL/s, and the nonresonant SHG signal at the solid/water interface and the background UV−vis spectrum prior to introducing the chromate solution were recorded. At the same incident power, we observed increased nonresonant background SHG signals for the siloxane-functionalized silica/water interfaces versus the nonfunctionalized silica/water interfaces. This could be due to the different interfacial dielectric constants in the presence and absence of the siloxane adlayers at the solid/water interface.[58] After recording the background signals from the interface and the bulk aqueous solution, the chromate solution flow was turned on at a given time using a Teflon on−off valve (Swagelok). The settings of the water pump were adjusted such that the total flow rate remained constant at 0.52 mL/s. The adsorption of chromate was monitored as an increase in the SHG signal intensity at a second harmonic wavelength of 290 nm. After reaching steady state, the chromate solution flow was turned off and the settings of the water pump were readjusted to maintain a constant flow rate of 0.52 mL/s. The concentration of the chromate solution in a typical experiment ranged from 1×10^{-6} to 1×10^{-4} M, and adsorption isotherms were recorded by starting with the lowest limit. The concentration of the chromate solution in the reservoir was increased after the completion of each adsorption/desorption cycle.

Details about the laser system used in these experiments have also been described previously.[50,51] Briefly, the system consists of a Ti:sapphire laser (kHz, 120 fsec, Hurricane, Spectra Physics) pumping an optical parametric amplifier (OPA-CF, Spectra Physics). The output light from the OPA at 580 nm was focused onto the aqueous/solid interfaces at an angle of 60° and a spot size approximately 50 μm in diameter and was used to monitor adsorbed Cr(VI) via a two-photon resonance centered around 290 nm. The enhancement of the SHG signal in the presence of Cr(VI) is consistent with the fundamental probe light being in resonance with ligand-to-metal charge-transfer transitions in the chromate ion.[51] After isolating the SHG signal from processes other than SHG via Schott filters and a monochromator, the SHG signal was collected using a single-photon counting system.

The recorded SHG intensity, I_{SHG}, is related to the second-order susceptibility of the interface, $\chi_{int}^{(2)}$.[59−61] When the SHG electric field, E_{SHG}, is resonantly enhanced, as in the case of adsorbed Cr(VI), $\chi_{int}^{(2)}$ consists of a nonresonant and a resonant contribution, $\chi_{NR}^{(2)}$ and $\chi_R^{(2)}$, respectively. If the resonant

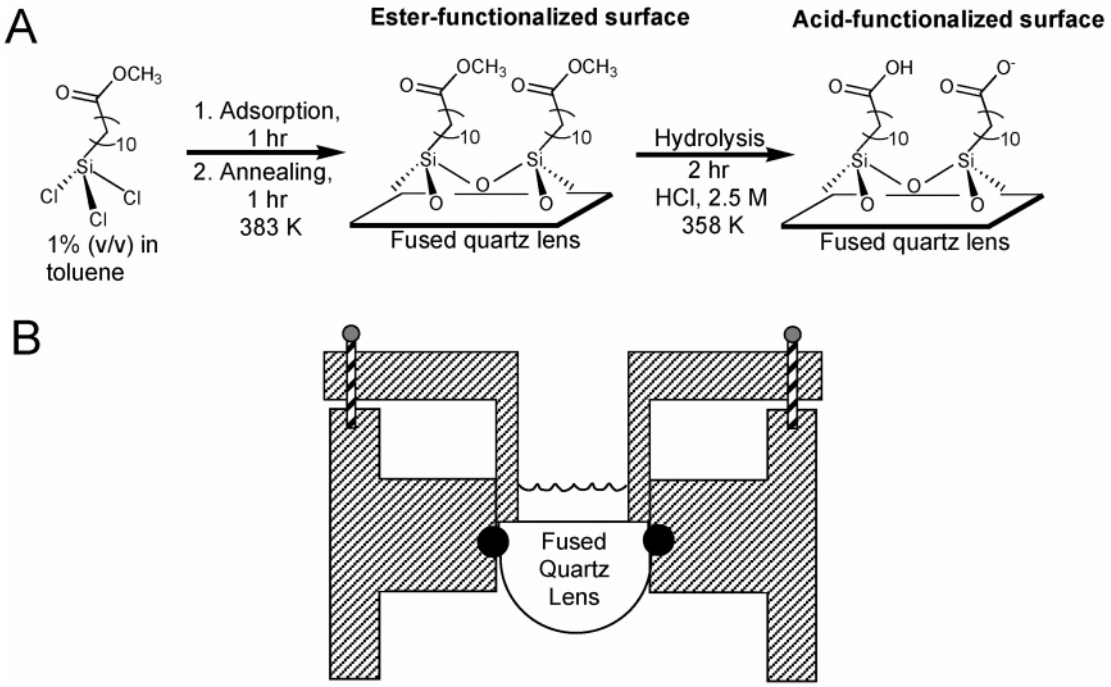

Figure 1. (a) Reaction scheme for preparing the siloxane adlayers on the fused quartz lens. (b) Cross-section of the custom-built Teflon cell used for depositing siloxane adlayers on the fused quartz lens.

contribution dominates, $\chi_R^{(2)}$ can be modeled as the product of the number density of molecules adsorbed on the surface and the molecular hyperpolarizability, $\alpha^{(2)}$, averaged over all molecular orientations, according to eq 1:

$$\sqrt{I_{SHG}} \sim \chi_{int}^{(2)} = \chi_{NR}^{(2)} + \chi_R^{(2)} = \chi_{NR}^{(2)} + N_{ads}\langle\alpha^{(2)}\rangle = E_{SHG} \quad (1)$$

Equation 1 shows that SHG can be used to perform thermodynamic and kinetic studies of heterogeneous processes by monitoring the concentration- and the time-dependence of the square root of the SHG intensity. In the above expression, the phase shift between the SHG E-field from the adsorbate and the one originating from the underlying substrate is assumed to be 0 or 180 degrees. The net SHG E-field originating from the adsorbate is thus obtained by taking the difference between the square root of the SHG signal intensity obtained from the interface with the adsorbate present and the square root of the SHG signal intensity obtained from the plain interface (no adsorbate present). It is important to note, however, that for a ninety-degree phase shift one should take the difference between the SHG signal intensity obtained from the interface with the adsorbate present and the one obtained from the plain interface (no adsorbate present), followed by taking the square root of that difference.

Formation and Characterization of the Siloxane Adlayers. A detailed description of the synthetic procedures for the organosilane solutions and the formation and characterization of the siloxane adlayers has been described previously.[48,62] Briefly, methyl ester-functionalized silanes, prepared as described in our previous work,[48,62] were freshly deposited on the fused quartz lens (Figure 1a). The lens was first washed in an ultrasonic methanol bath for five minutes, allowed to dry in ambient air, and then transferred to a plasma cleaner chamber (Harrick) operated in air at high power for 15 min. Afterward, the lens was placed in a custom-built Teflon cell (Figure 1b), which holds the lens leak-tight, exposing the center area of the flat surface for siloxane adlayer deposition while protecting the rest of the lens from exposure to the organosilane solution. The deposition of the ester-terminated siloxane adlayers was carried out in an inert atmosphere glovebox by covering the exposed area of the fused quartz lens with about 2 mL of 1% (v/v) of 1-(trichlorosilyl)-11-carbomethoxyundecane in toluene for 1 h, after which excess solution was washed out several times with toluene followed by methanol. After deposition, the siloxane adlayers were annealed for 1 h at 383 K to facilitate rigid cross-linking of the adlayers.[63] Ester-functionalized surfaces were stored in a closed beaker in air and rinsed with methanol twice before bringing them in contact with the aqueous phase in the flow cell. For the preparation of carboxylic acid-terminated siloxane adlayers, the ester-functionalized surfaces were immersed in 2.5 M HCl at 358 K for 2 h. Upon cooling to room temperature, carboxylic acid-functionalized surfaces were rinsed with Millipore water several times and stored in a beaker filled with Millipore water held at neutral pH. Detailed characterization studies of these siloxane adlayers can be found elsewhere.[48,62]

III. Results and Discussion

1. Adsorption Isotherms. Figure 2A shows 10 representative time traces of the square root of the SHG intensity, i.e., the SHG E-field, at $\lambda_{SHG} = 290$ nm as a function of increasing bulk chromate concentration for chromate binding to ester-functionalized surfaces in the submonolayer coverage regime and at pH 7.0(2). Here, the number in parentheses represents the error associated with the preceding value. Figure 2B shows a selected number of UV−vis absorbance spectra of the bulk chromate solutions at various chromate concentrations, which were recorded simultaneously with the SHG data. The SHG E-field vs time traces were smoothed by slide averaging every three consecutive data points in SHG counts and time. For all the SHG vs time traces shown, the chromate flow was turned on at 180 s, and it took 39(2) seconds for the chromate to reach the Teflon flow cell. For a given chromate concentration, the SHG E-field increases when the chromate flow is turned on and reaches a constant, steady-state level. After turning off the

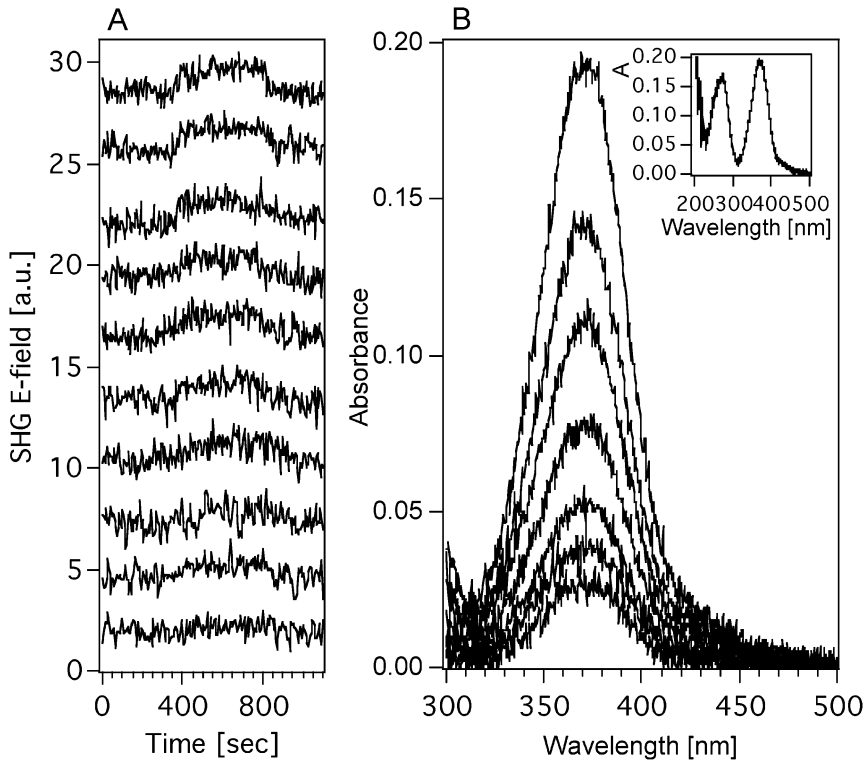

Figure 2. (A) Time traces of the square root of the SHG intensity at $\lambda_{SHG} = 290$ nm for chromate adsorption on ester-functionalized silica/water interface recorded as a function of increasing bulk chromate solution concentration in the submonolayer regime at pH 7 and 300 K, from bottom to top ($\times 10^{-5}$ M): 0.81, 0.88, 1.1, 1.7, 1.9, 2.1, 2.4, 2.6, 3.0, and 4.1. Data shown is smoothed by slide averaging clusters of three consecutive raw data points in both time and intensity. (B) Selected bulk UV−vis absorption spectra of the lower energy ligand-to-metal charge transfer band of aqueous chromate solutions recorded simultaneously with the SHG measurements shown in Figure 2A. Spectra are recorded for the effluent stream exiting the flow cell. Inset: Bulk chromate absorption spectrum between 210 and 500 nm. All data recorded at a pH of 7.2.

chromate solution flow, the SHG E-field decreases to its original background level, indicating that the binding of chromate to the ester-functionalized silica/water interfaces is reversible. A similar behavior was observed for chromate binding to the carboxylic acid-functionalized silica/water interface. The reversible nature of chromate binding to siloxane adlayers suggests that a physisorption process, which is discussed in detail below, governs the interaction of chromate with these functionalized surfaces.

Figure 2 also shows that the net SHG signal gain due to chromate adsorption increases with increasing chromate concentration in the bulk solution flowing over the interface. When comparing the SHG signal intensities obtained from the various surfaces under investigation at constant laser input power and in the presence of adsorbed Cr(VI), we found that the magnitude of the SHG signal increase due to chromate adsorption to the siloxane-functionalized silica/water interfaces is consistently less than that observed for the nonfunctionalized silica/water interfaces. This is shown in Figure 3, where the power- and background-normalized SHG E-field vs traces are shown for chromate interaction with the silica/water interface (trace A), the carboxylic acid-functionalized interface (trace B), and the methyl-ester functionalized interface (trace C). The chromate concentration in these experiments was around 3×10^{-5} M. The lower SHG E-field gain observed for chromate interaction with the functionalized interfaces is expected since each silane molecule used in the organic adlayer deposition process consumes a maximum of three SiOH groups on the silica surface. Hence, the total number of sites available for chromate adsorption to the siloxane-functionalized surfaces is lower than that of the nonfunctionalized silica surfaces, which is consistent with the data shown in Figure 3.

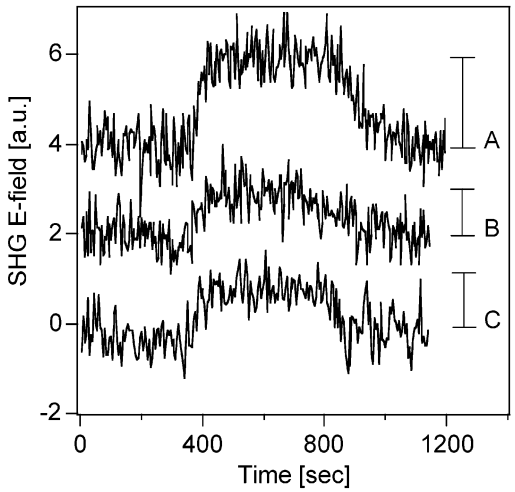

Figure 3. SHG E-field vs time traces of chromate interacting with a silica/water interface (A, no siloxanes present), with a carboxylic acid-functionalized silica/water interface (B), and with a methyl ester-functionalized silica/water interface (C). Data offset for clarity. The bars on the right indicate the net signal increase due to resonantly enhanced SHG, which is proportional to the Cr(VI) surface coverage. All data recorded using chromate concentrations near 3×10^{-5} M and at a pH of 7.2.

Adsorption isotherms for the interaction of chromate with the acid- and the ester-functionalized silica/water interfaces were measured at pH 7.0(2) and room temperature. For each chromate adsorption/desorption experiment conducted on the freshly prepared siloxane adlayers, the relative Cr(VI) surface coverage was determined by subtracting the nonresonant contribution to the SHG E-field prior to flowing chromate from the resonant

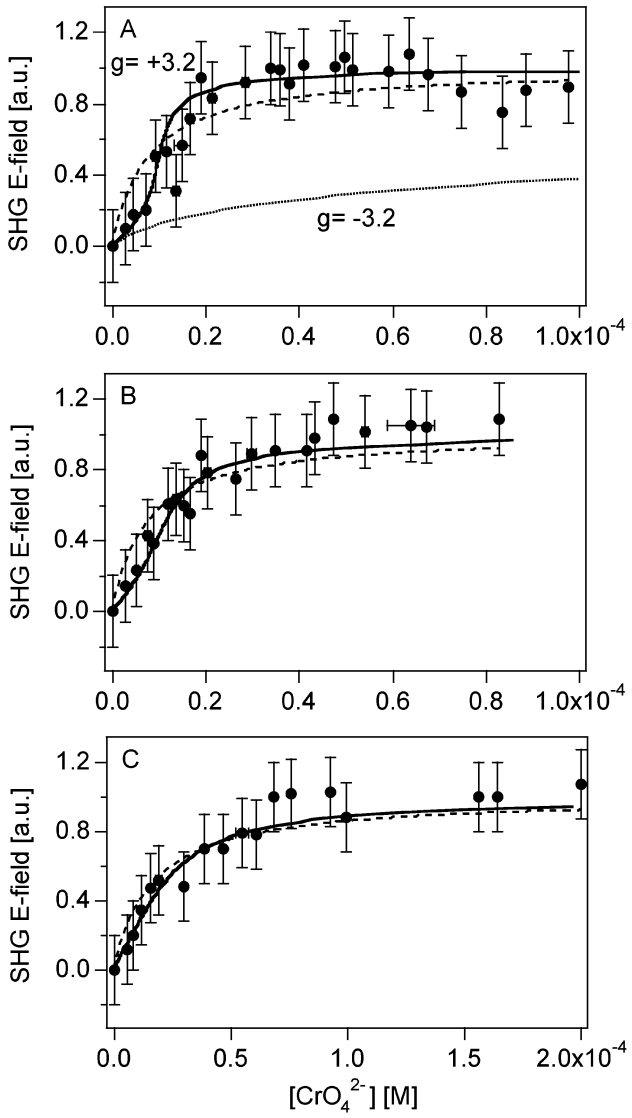

Figure 4. Adsorption isotherms of chromate measured at pH 7 and 300 K on (A) carboxylic acid-functionalized, (B) ester-functionalized, and (C) nonfunctionalized silica/water interfaces. Experimental data (filled circles) is normalized to the maximum SHG field obtained in the monolayer regimes. Each isotherm represents a composite of two separate experiments on two freshly prepared surfaces for each interface. The solid lines through the data represent the fit of the FFG model to the data. The dashed lines represent the fit of the Langmuir model to the data. The dotted line in Figure A represents the fit of the FFG model to the data using a g value of -3.2, which corresponds to repulsive lateral adsorbate−adsorbate interactions. All data recorded at a pH of 7.2. See text for details.

contribution (eq 1). Data points were then normalized to the SHG E-field obtained in the monolayer regime, such that quantitative comparisons between experiments conducted on different days with different samples of the same organic adlayers could be established.

Figures 4A and 4B show isotherms for chromate adsorption to the carboxylic acid-, and the ester-functionalized silica/water interfaces at pH 7.0(2) and 300 K, respectively. For comparison, Figure 4C shows chromate adsorption isotherm to the nonfunctionalized silica/water interface (no siloxanes present) under the same conditions. Data shown in Figure 4 are the composite of several runs performed on two freshly prepared samples. The error bars are taken as the largest standard deviation obtained when averaging SHG E-fields recorded at approximately the same chromate concentration. All three adsorption isotherms appear to be limited to a monolayer of adsorbed Cr(VI), which sets in at about $2-3 \times 10^{-5}$ M for the functionalized surfaces and at about $5-10 \times 10^{-5}$ M for the plain silica surface (no siloxanes present).

2. Thermodynamic Analysis of the Adsorption Isotherms. In contrast to the chromate adsorption isotherm recorded for the nonfunctionalized silica/water interface (no siloxanes present), the adsorption isotherms recorded for the functionalized silica/water interfaces show curvature in the submonolayer coverage regime. This observation is consistent with the notion that cooperative effects, possibly mediated by adsorbate−adsorbate interactions, are important in the interaction of chromate with the functionalized surfaces.[64,65]

It is important to note that the organic functional groups are mainly neutral under the experimental conditions employed in this work: the ester-functionalized surface is not expected to exhibit acid/base behavior. The carboxylic acid-functionalized surface, in contrast, should exhibit acid−base behavior, which we studied using direct, surface-specific $\chi^{(3)}$ measurements of the interfacial charge density for carboxylic acid functionalized silica/water interfaces.[49] At pH 7, it was found that less than 5% of the terminal −COOH groups of the acid-functionalized surfaces are in the deprotonated state. The remaining 95% of the adlayer consists of neutral carboxylic acid groups that are energetically stabilized by lateral hydrogen bonds between the carboxylic acid groups. Thus, we can consider the carboxylic acid functionalized silica/water interface to be mainly neutral at pH 7, where the chromate adsorption studies were carried out.

Given the S-shape of the adsorption isotherms carried out on the organic-functionalized surfaces, we analyzed them using two common adsorption models: the standard Langmuir model and a modified Langmuir model, specifically, the Frumkin−Fowler−Guggenheim adsorption model, which introduces a coverage-dependent adsorption equilibrium constant to the standard Langmuir adsorption model.

A. Standard Langmuir Model. First, the standard Langmuir adsorption model is used to fit the experimental data shown in Figure 4.[66] The experimental data were used to generate linear plots of $1/\theta$ versus $1/[CrO_4^{2-}]$ for the submonolayer regime to extract the fit parameters.[51] The inverse of the slope obtained from the linear least-squares fit is given by eq 2:[65]

$$\left(\frac{d(1/\theta)}{d(1/[CrO_4^{2-}])}\right)^{-1} = \frac{1}{55.5\ \mathrm{M}} \exp(\Delta G^\circ_{ads}/RT) = K(\mathrm{M}^{-1}) \quad (2)$$

Equation 2 is used to calculate the equilibrium constant for chromate adsorption, K_{ads}, which is referenced to the molarity of water in the aqueous solution (55.5 M).[65] From the equilibrium constant for chromate adsorption, the corresponding standard free energy of adsorption, ΔG°_{ads}, is obtained. The fits of the standard Langmuir model to the isotherm data are shown as the dashed lines in Figure 4. The values for the equilibrium adsorption constants for the carboxylic acid-functionalized, the ester-functionalized, and the nonfunctionalized silica/water interfaces are found to be $2.1(2) \times 10^6$, $3.2(2) \times 10^6$, and $1.2(2) \times 10^6$, again referenced to the molarity of the aqueous solution under standard conditions (55.5 M). The resulting values for ΔG°_{ads} calculated for chromate adsorption to the carboxylic acid-functionalized, the ester-functionalized, and the nonfunctionalized silica/water interfaces are found to be 36.4(2), 37.3(1), and 35.0(3) kJ/mol at pH 7 and 300 K, respectively. These thermodynamic results are summarized in Table 1.

TABLE 1: Summary of Results Obtained from Fitting Adsorption Models to Chromate Adsorption Isotherm Measurements at 300 K and pH 7[a]

	Langmuir model			FFG model	
interface	K_{ads}	$\Delta G°_{ads}$ [kJ/mol]	g	K_{ads}	$\Delta G°_{ads}$ [kJ/mol]
carboxylic acid-terminated siloxane	$2.1(2) \times 10^6$	36.4(2)	3.2(2)	$1.1(1) \times 10^6$	34.7(3)
methyl ester-terminated siloxane	$3.2(2) \times 10^6$	37.3(1)	2.1(2)	$1.9(2) \times 10^6$	36.1(3)
silica (no siloxane present)	$1.2(1) \times 10^6$	35.0(3)	1.3(2)	$1.3(8) \times 10^6$	35.2(2)

[a] Equilibrium constants are referenced to the molarity of water under standard conditions (55.5 M).

B. Frumkin−Fowler−Guggenheim (FFG) Model. Some of the assumptions in the Langmuir model are that the surface is energetically homogeneous and that the adsorption energy is independent of surface coverage.[65] While this model seems to describe the general features of the experimentally obtained isotherm on the nonfunctionalized silica/water interface (no siloxanes present), it does not accurately describe the submonolayer regime of the chromate adsorption isotherms for the ester- and the acid-functionalized surfaces. For example, Figure 4A shows that at low chromate concentrations, the Cr(VI) surface coverage is below that expected from the standard Langmuir model, and starts to increase rapidly at higher chromate concentrations until a monolayer is formed. A general interpretation of such S-shaped adsorption isotherms, which are commonly found in geochemical applications involving organic compounds,[2] is that surface-bound species increase the adsorption affinity of a surface through cooperative effects, which can be direct or indirect in nature,[64] until a monolayer is reached. We will discuss specific aspects of this interpretation in the context of the siloxane adlayers below.

To account for the increased adsorption affinity of the functionalized silica/water interfaces toward Cr(VI), we applied the Frumkin−Fowler−Guggenheim (FFG) adsorption model, which uses a second fitting parameter that describes a coverage-dependent equilibrium adsorption constant. The FFG model, also known as the Fowler adsorption model,[64] is a modified version of the Langmuir model that describes the S-shaped isotherm observed in Figures 4A and 4B by introducing the surface coverage-dependent factor $e^{-g\theta}$ into the simple Langmuir equation:[2,64,65]

$$\frac{\theta}{1-\theta}e^{-g\theta} = K_{ads}[CrO_4^{2-}], \quad g = \frac{zu}{RT} \tag{3}$$

Here, z is the number of the nearest-neighbor adsorption sites, u is the interaction energy between two adsorbates on two nearest-neighbor adsorption sites, K_{ads} is the adsorption equilibrium constant in the limit of an infinitely small surface coverage, $[CrO_4^{2-}]$ is the chromate concentration in solution, R is the universal gas constant, and T is the temperature in Kelvin. Equation 3 shows that the equilibrium adsorption constant varies with Cr(VI) surface coverage according to $K(\theta) = K_{ads}e^{g\theta}$,[67] where K_{ads} is the equilibrium adsorption constant in the limit of infinitely small surface coverage. In general, the interaction energy u is positive for attractive or stabilizing interactions and negative for repulsive lateral or destabilizing interactions.[2]

Equation 3 can be used to fit the experimental data shown in Figure 4 after extracting the interaction parameters g and K_{ads} from the fit. The fit parameters can be obtained by rearranging eq 3 into the linear form:

$$\ln\left(\frac{\theta}{1-\theta}\right) - g\theta = \ln K_{ads} + \ln[CrO_4^{2-}] \tag{4}$$

The experimental data in the submonolayer regime is used to generate plots of $\ln[\theta/(1-\theta)] - g\theta$ versus $\ln[CrO_4^{2-}]$ while adjusting the energy parameter g until a straight line with a slope of near unity is obtained. The y-intercept is then referenced to the molarity of water in the aqueous solution (55.5 M)[65] and used to calculate the standard free energy of adsorption, $\Delta G°_{ads}$. Using eq 4, the best fit to the data for the carboxylic acid-functionalized silica/water interface is given as the solid line in Figure 4A and was obtained with a g value of 3.2(2). The error in g stems from constraining the data range used in the fit to submonolayer regimes representing 75 to 90% of a monolayer. The fit results in a $\Delta G°_{ads}$ of 34.7(3) kJ/mol, which corresponds to an equilibrium constant for chromate adsorption of $1.0(3) \times 10^6$, again referenced to the molarity of water in the aqueous solution under standard conditions. The interaction energy, u, ranges from 1.3 to 8.0 kJ/mol, assuming a range of next neighbors, z, between 6 and 1, respectively. For comparison, the result of a fit of eq 4 to the isotherm data using a negative value for g, which would correspond to destabilizing lateral adsorbate−adsorbate interactions, is shown as the dotted line in Figure 4A. It can be seen that this fit grossly undershoots the isotherm data.

For the ester-functionalized silica/water interface, we obtained a g value of 2.1(2) and free energies and equilibrium constants of adsorption that are similar to those found for the carboxylic acid-functionalized silica/water interface. For the silica/water interface, a g value of 1.3(2) was found, which is consistent with the small curvature in the adsorption isotherm. Again, adsorption free energies and equilibrium constants are similar to those found for the functionalized silica/water interfaces. The results from our thermodynamic analysis are summarized in Table 1. The similarities in adsorption free energies and equilibrium constants across the three systems are not surprising, as the interaction of chromate with these interfaces is most likely dominated by hydrogen bonding.

As stated in the SHG background section, a phase shift of 90 degrees results in a different background subtraction procedure than a 0 or 180 degree phase shift. We thus carried out this second background subtraction procedure for obtaining the net increase in the SHG E-field due to chromate adsorption. Figure 5 shows a Cr(VI) adsorption isotherm on a carboxylic acid-functionalized silica/water interface, obtained by using the two different background subtraction schemes applied to a chromate adsorption isotherm measurement carried out at pH 7 and room temperature. The empty circles show the case for taking the difference in the square root of the SHG signal intensities (phase shift of 0 or 180 degrees), and the filled circles show the case for taking the square root of differences in the SHG signal intensities (phase shift of 90 degrees). The dashed line is the Langmuir model fit and the solid and dotted lines are the FFG model fits to the data. When compared to the 0 or 180 degree phase shift case, the submonolayer data points for the 90 degree phase shift to higher values. The FFG model fit yields g parameters of +3.2 and +3.6 for the 90 and the 0 or 180 degree phase shift case, respectively, while the equilibrium

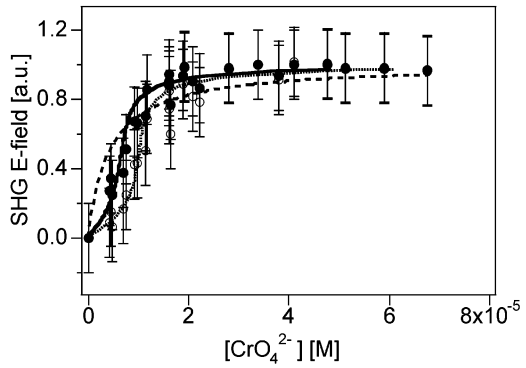

Figure 5. Cr(VI) adsorption isotherm on a carboxylic acid-functionalized silica/water interface, obtained by using two different background subtraction schemes that assume SHG phase shifts of zero or 180 degrees (empty circles) and ninety degrees (filled circles). The dashed line is the Langmuir model fit and the solid and dotted lines are the FFG model fits to the data. All data recorded at pH 7 and room temperature. See text for details.

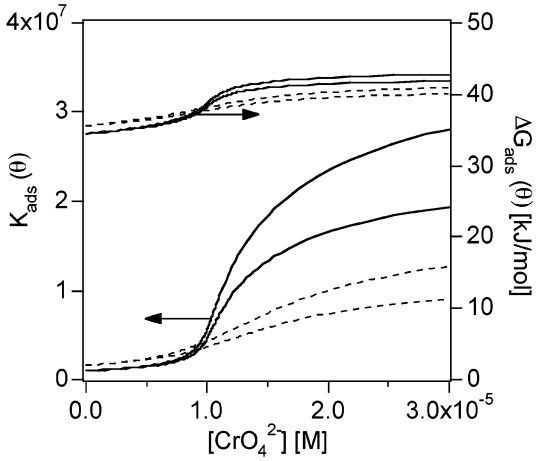

Figure 6. Dependence of the adsorption equilibrium constant and free energy on chromate concentration in bulk solution for chromate adsorption on the acid- and the ester-functionalized surfaces.

adsorption constants for the two cases are found to be $1.7(1) \times 10^6$ and $0.89(6) \times 10^6$, referenced to the molarity of the aqueous solution under standard conditions. The equilibrium adsorption constants correspond to free adsorption energies of 34.2(3) kJ/mol and 35.8(3) kJ/mol for the two background subtraction procedures. This case study thus shows that the phase shift between the SHG E-field from the adsorbates and phase shift from the underlying organic adlayer have a minor effect on the *g* parameters and no appreciable effect on the thermodynamic parameters obtained from the FFG model fits. In future work, we will, however, measure the absolute phases of both SHG E-fields referenced to *z*-cut quartz.

Using our fit parameters, we can calculate the dependence of the adsorption equilibrium constant and the free energy on the chromate bulk concentration in the range corresponding to the submonolayer regime. We included the uncertainties in *g* and in K_{ads} for each interface (Table 1), and the results are shown in Figure 6. Here, the resulting ranges in the adsorption equilibrium constants, referenced to the molarity of the aqueous solution (55.5 M), are plotted as a function of chromate concentration for the carboxylic acid- (bottom set of solid lines) and the ester-functionalized surfaces (bottom set of dashed lines). The corresponding dependence of the free energy of adsorption is plotted in the top set of black and dashed lines for the carboxylic acid- and the ester-functionalized surfaces, respectively. It can be seen that the adsorption equilibrium constant and the free energy increase with increasing chromate concentration.

C. Direct and Indirect Surface Effects. Clearly, adsorbate−adsorbate interactions are important in the interaction of chromate with the interfaces containing the organic adlayers. In general, these effects can be either direct or indirect.[64] Direct effects can be attributed to the lateral interaction of two or more adsorbed species, which could be mediated by dipole−dipole and/or ion−dipole interactions or the presence of counterions. The floppiness of the siloxane carbon backbones, which contain 10 methylene groups underneath the functional end group and which are likely to undergo randomized motion within the interfacial layer, may facilitate such lateral interactions among the adsorbed species. Our SHG measurements would thus represent the time- and spatial average of such lateral adsorbate−adsorbate interactions. Indirect effects that can account for the curvature of the adsorption isotherms in the submonolayer regime could stem from hydrogen bonding between water molecules in the tightly bound chromate solvation sphere and the organic functional groups, which could lower the effective electron density within the surface layer (including already surface-bound Cr(VI) ions). This scenario would result in a higher affinity of the functionalized silica/water interfaces toward the 2-fold negatively charged chromate anion in solution. However, due to the fact that the organic adlayers and the underlying fused silica substrate are high-band gap materials, indirect effects are unlikely to be important here.

The stabilizing lateral adsorbate−adsorbate interactions that are obtained from the FFG analysis of the adsorption isotherms suggest that the negative charge on the chromate anion is efficiently screened by the counterions and solvating water molecules around the chromate anion such that attractive lateral adsorbate−adsorbate interactions dominate Coulombic repulsion of adsorbed Cr(VI) species. Thus, including solvent reorganization, the energy sum for the "effective" adsorbate−adsorbate interactions may be expressed as

$$u = u_{\text{rep}} + u_{\text{ion-dipole}} + u_{\text{dipole-dipole}} \tag{5a}$$

Here, *u* represents the interaction energy and the subscripts refer to destabilizing Coulomb repulsion among adsorbed Cr(VI) anions, ion−dipole, and dipole−dipole stabilizing interactions, respectively. With positive *g* values, i.e., stabilizing overall lateral interaction energies, it follows that

$$|u_{\text{rep}}| < |u_{\text{ion-dipole}} + u_{\text{dipole-dipole}}| \tag{5b}$$

The notion that Coulomb repulsions among anions adsorbed at aqueous interfaces can be overcome by stabilizing ion−dipole and dipole−dipole interaction and/or the presence of counterions within the interfacial layer is consistent with recent reports indicating that polarizable anions can preferentially bind to aqueous surfaces and interfaces.[68−71] In addition, anion adsorption can lead to changes in the water structure within the interfacial region, as has been recently shown by a number of nonlinear optical and molecular dynamics studies.[68,69,72−74] For example, vibrational sum frequency spectra in the OH stretching region show that inorganic anions can disrupt the interfacial hydrogen bonding network,[73] and decrease the number density of free, or "dangling" OH groups at the air−water interface.[68,69]

The free energies of adsorption, ΔG°_{ads}, and the stabilizing *g* values obtained from fitting the FFG model to the isotherm data indicate that the interaction of the surface with chromate is dominated by two parameters: (a) hydrogen bonding between

SCHEME 1: Deconstruction of the Overall Free Energy of Adsorption into Adsorbate−Surface Interactions and the "effective" Lateral Adsorbate−Adsorbate Interactions for Chromate Binding to the Carboxylic Acid-functionalized Silica/Water Interface[a]

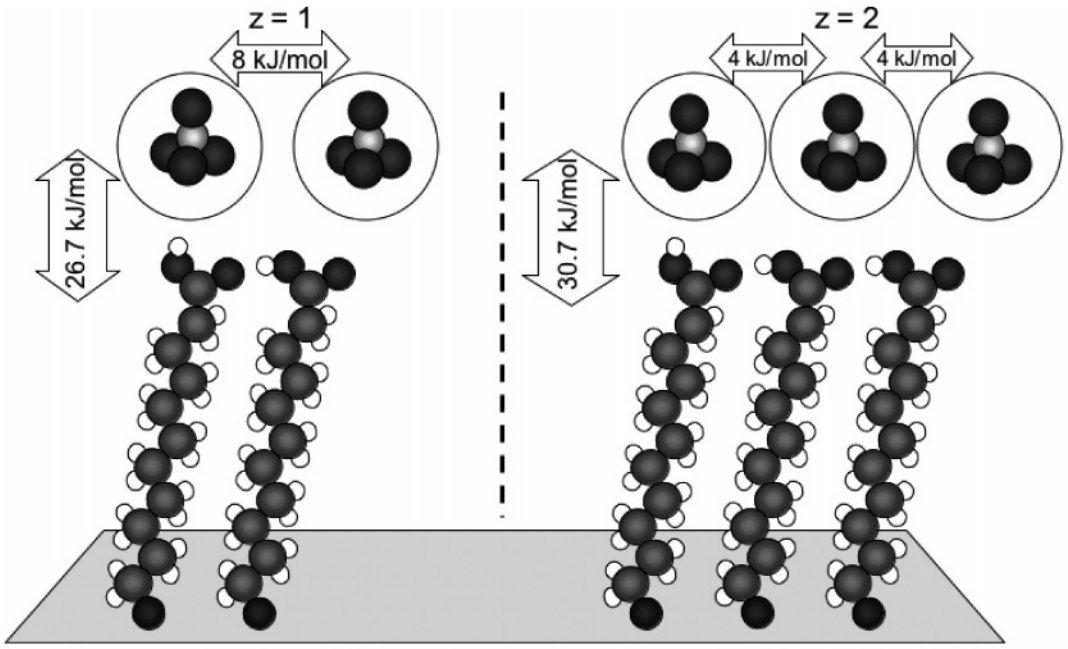

[a] The number of nearest neighbors is assumed to be one (left) or two (right). Vertical arrows indicate the magnitude of the interaction free energy between adsorbed Cr(VI) and the organic functional groups; horizontal arrows indicate the free energy of the stabilizing lateral interactions. The circles around the chromate symbolize the solvent solvation sphere, including counterions.

the surface and the adsorbates, and (b) lateral adsorbate−adsorbate attraction mediated by water molecules and counterions in the adsorbate solvation sphere, whose energy is on the order of dipole−dipole or ion−dipole interaction energies. As such, an understanding of the lateral interaction energies allows us to deconstruct the overall free energy of adsorption into adsorbate−surface interactions and lateral adsorbate−adsorbate interactions. This is depicted in Scheme 1 for the carboxylic acid-functionalized silica/water interface. Here, the vertical arrows represent hydrogen bonding between adsorbed Cr(VI) and the organic functional groups, and the horizontal arrows indicate lateral dipole−dipole or ion−dipole interactions. With a g value of 3.2, and assuming that the number of nearest neighbors is limited to one (left) or two (right), the lateral interaction energies are 8.0 and 4.0 kJ/mol, respectively.

It is important to note that while the stabilizing interactions are typically treated as enthalpies in gas−solid systems,[64] the experiments presented in this work are carried out in aqueous solution and include solvent reorganization upon adsorption of the Cr(VI) anion. The "effective" stabilizing interaction energies may thus be treated as free energies. With an overall free energy of adsorption of 34.7 kJ/mol for the carboxylic acid-functionalized surface, and with lateral (horizontal) adsorbate−adsorbate interaction free energies ranging from 8.0 to 4.0 kJ/mol for the case of one or two nearest neighbors, respectively, we calculate the free energy for the (vertical) adsorbate−surface interaction to be 26.7 kJ/mol in the case of one nearest neighbor ($z = 1$) and 30.7 kJ/mol in the case of two nearest neighbors ($z = 2$). These (vertical) adsorbate−surface energies are consistent with the notion that the interaction of Cr(VI) with the functionalized surfaces occurs via hydrogen bonding. Temperature-dependent studies are planned with the goal to obtain isosteric heats of adsorption as well as adsorption entropies.

3. Adlayer Stability in the Presence of Cr(VI). While recording the adsorption isotherms on the siloxane-functionalized silica/water interfaces using chromate concentrations corresponding to monolayer coverages, a decrease in the SHG signal was observed for chromate concentrations higher than 1×10^{-4} M. This is shown in Figure 7A, where the filled circles show the SHG E-field for an acid-functionalized silica/water interface recorded as a function of increasing chromate concentration up to 2.5×10^{-4} M. The observed signal decay could be due to a decrease in the stability of the siloxane adlayer at these chromate concentrations, or due to prolonged exposure of the interface to Cr(VI), independent of concentration, or both.

Cr(VI) is a well-known oxidizer of organic compounds under acidic reaction conditions.[75] In general, organic reactions involving Cr(VI) can involve radicals,[42,76] which in our case could result in the formation of organic polymers with a low binding affinity toward Cr(VI). This would be consistent with the observed SHG signal decrease. Even though the chromate concentrations used in this study were all below 3×10^{-4} M, and thus well below the chromate concentrations commonly used in organic oxidation reactions,[42,43] and even though the pH employed in our experiments is neutral, we set out to examine the stability of the organic adlayers in the presence of Cr(VI), specifically its time- and concentration-dependence. Such stability studies are highly relevant to understanding the deleterious effects of Cr(VI) in the human body, where prolonged exposure to Cr(VI) commonly leads to cell death and hemorrhaging before cancers develop.[9]

Figure 7B shows the effect of chromate exposure time on the stability of an acid-functionalized silica/water interface in the presence of an adsorbed Cr(VI) monolayer. The filled squares in Figure 7B show the SHG signal intensity during a continuous 2-h exposure of the interface to chromate at a high concentration of 1.7×10^{-4} M. A decrease in the SHG signal was observed to occur within 30 min of exposure to chromate, and this decrease continued throughout the course of the experiment. This initial time period of 30 min corresponds to

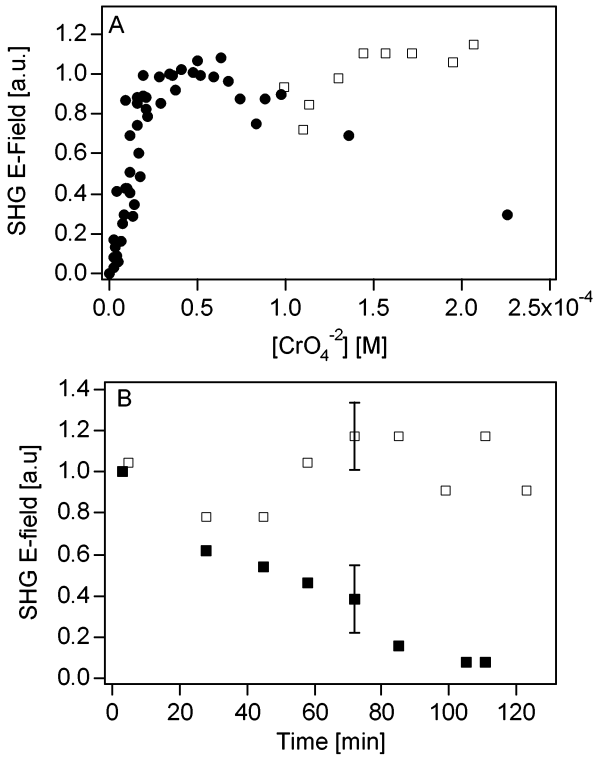

Figure 7. Stability of the carboxylic acid-functionalized surfaces due to exposure to chromate solution at pH 7 and 300 K. (A) Filled circles: Decay of the SHG signal intensity is observed for bulk chromate solution concentrations greater than 1×10^{-4} M. Empty squares: Control experiment using chromate concentrations resulting in monolayer Cr(VI) coverages and a total exposure time under 30 min. (B) SHG signal intensity during to consecutive exposure of the carboxylic acid-functionalized surface to chromate during nine adsorption/desorption cycles with a total exposure time below 30 min ($[CrO_4^{2-}] = 1.5 \times 10^{-4}$ M, empty squares), and continuous exposure to chromate solution ($[CrO_4^{2-}] = 1.7 \times 10^{-4}$ M, filled squares). All data recorded at a pH of 7.2. See text for details.

the cumulative Cr(VI) exposure time during collection of a single adsorption isotherm, after which the SHG signal decrease is observed.

The empty squares in Figure 7B show the results of a control experiment, in which an acid-functionalized silica/water interface was exposed to a similarly high chromate concentration (1.5×10^{-4} M) in consecutive four-minute long adsorption−desorption cycles. The cumulative exposure time in this experiment is approximately 35 min. Within experimental error, we did not observe a decrease in the SHG signal over the course of the experiment, indicating that the concentration of the chromate solution used in the adsorption isotherm experiments does not play a significant role in damaging the organic adlayer. Given this result, we collected additional data points for the chromate adsorption isotherm on an acid-functionalized silica/water interface using chromate concentrations between 1×10^{-4} and 2×10^{-4} M. In these experiments, the cumulative Cr(VI) exposure time was limited to less than 30 min. The results are shown as the empty squares in Figure 7A, which indicate that the SHG signal in the monolayer regime remained stable within experimental error, confirming the control experiments described above. Our experiments thus suggests that damage of the organic adlayer can be caused by exposing the interface to chromate for prolonged periods of time, i.e., degradation of the organic adlayers becomes important at long exposure times but is not a function of the chromate concentrations used in our experiments. Consistent with these results, the SHG signal remained stable within chromate concentrations corresponding to Cr(VI) monolayer surface coverages for the nonfunctionalized silica/water interface (no siloxane present, see Figure 4C) up to 2.5×10^{-4} M. Thus, one can conclude that damage of the interface does not occur until the cumulative Cr(VI) exposure time exceeds 30 min.

IV. Possible Environmental Implications

Assessing the mobility of pollutants in the environment represents a major challenge in environmental research. A parameter that is often included in chemical transport models is the retardation factor, R, which can be given by

$$R = 1 + (\rho/n)\mathrm{Kd} \qquad (6)$$

Here, ρ is the bulk density of the geosorbent, n is its porosity, and Kd represents the partition coefficient between the solution and the interface and describes the interaction of the sorbent with the solute. The Kd parameter is often taken from the initial slope of adsorption isotherms, and we have applied this method in the past to assess the mobility of chromate ions in silica-rich soil environments. Consistent with the high mobility of chromate in most soils,[9,35,52−57] we found a less than 10% decrease in the chromate mobility in silica-rich soil environments when compared to free-flowing groundwater.

As soil particles often contain a complex matrix of inorganic and functional organic compounds as surface adlayers, this matrix is the primary controller in the processes that control chemical binding of pollutants.[1−5] In this work, we have begun to address how surface-bound organic functional groups commonly found in surface-active biopolymers, specifically carboxylic acid and ester groups, impact the mobility of Cr(VI). Given the S-shaped adsorption isotherms found for the organic adlayers at the functionalized silica/water interfaces, the determination of Kd parameters from the initial slopes of the adsorption isotherms is problematic. However, the thermodynamic parameters obtained from the FFG model (vide supra) allow us to develop a chromate concentration-dependent parametrized expression for Kd and thus the retardation factor R.

When constraining linear fits of the isotherm data presented in Figure 4 were constrained to a chromate concentration of 1.9×10^{-5} M, the initial slope of the adsorption isotherm data for all three substrates yields Kd values of 0.01(1), 0.009(10), and 0.007(1) mL/g for the carboxylic acid-, the ester-, and the nonfunctionalized silica/water interfaces. Similar results are obtained when we constrain the linear fits of the isotherm data presented in Figure 4 to a Cr(VI) surface coverage of 50%: the initial slopes of the adsorption isotherm data yield Kd values of 0.011(2), 0.011(1), and 0.007(1) mL/g for the carboxylic acid-, the ester-, and the nonfunctionalized silica/water interfaces, respectively. For each substrate, we assumed the same number of Cr(VI) species per unit area, namely 1×10^{14} ions per cm^2, which represents an upper limit. The variables in the adsorption isotherms were transformed according to our previous work[50] to yield Kd values in the units of mL/g. The Kd value for the silica/water interface agrees well with the one obtained in our previous work[50] and indicates high chromate mobility in most silica-rich soils. Using typical soil densities and porosities (yielding ρ/n ratios between 4 and 10),[6] the corresponding retardation factors (for all substrates) vary between 2 and 10% with respect to the free-flowing groundwater phase.

It is important to note that the FFG parametrization of the equilibrium adsorption constant $K(\theta)$ (Figure 6) is valid for the submonolayer coverage regime, i.e., the surface coverage range where θ changes with the concentration of chromate ions in

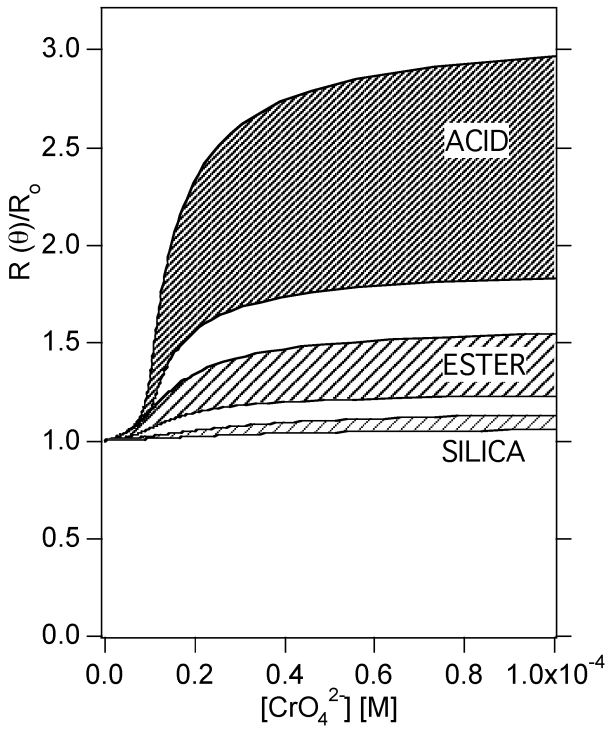

Figure 8. Parametrized chromate retardation factor relative to the nonparametrized chromate retardation factor as a function chromate concentration in bulk solution for the carboxylic acid-, the ester- and the nonfunctionalized silica/water interface at pH 7.

the bulk. This is also the regime where the Kd model is often applied. Thus, the g values obtained for the different surfaces under investigation in this work can be used to parametrize the Kd expression by multiplying the Kd values obtained from the initial slopes of the experimental isotherms with the factor $\exp(g\theta)$, i.e., $\mathrm{Kd}(\theta) = \mathrm{Kd} \times \exp(g\theta)$. Here, the g value is obtained from the thermodynamic analysis of the adsorption isotherms (vide supra), and θ is the relative Cr(VI) surface coverage on the particle surface. The FFG parametrization presented here is based on the fact that the Kd value is directly related to the equilibrium constant for adsorption, $K(\theta)$,which we have shown in this work to depend on the Cr(VI) surface coverage.

To calculate the Cr(VI) surface coverage-dependence that is necessary for the FFG parametrization of $\mathrm{Kd}(\theta)$, eq 3 was used with the appropriate thermodynamic parameters for each interface (Table 1) to generate data pairs of relative surface coverage and bulk chromate concentration. The Cr(VI) surface coverage on the various adlayers was then multiplied by the g value for each interface, and the resulting $(g\theta)$ exponent was used to calculate the $\mathrm{Kd}(\theta)$ value for each relative surface coverage between 0 and 1. Using typical values for the soil density divided by the porosity (between 4 and 10), the corresponding retardation factors are calculated according to eq 6.

Figure 8 shows how the ratio of the retardation with and without a coverage-dependent Kd value, i.e., $R(\theta)/R_o$, depends on Cr(VI) surface coverage. It can be seen that the retardation factor for the carboxylic acid-functionalized surfaces (solid line) can be up to three times higher when coverage dependence is included in the model. Likewise, the retardation can increase by a factor of 1.5 in the case of the ester-functionalized surface (dashed line). Including the low g value of 1.3 from the chromate adsorption isotherm carried out on the silica/water interface in this model results in an increase of chromate retardation of only 6 to 15%. These predictions are consistent with other laboratory studies,[77,78] which show that the mobility of chromate in organic-rich soils is often reduced relative to silica-rich soils with a low content of organic compounds (changes in surface area may contribute to this effect as well). Furthermore, our model shows that carboxylic acid groups, which are ubiquitous in humic and fulvic acids, may lead to a higher retardation than the less common methyl ester functional groups. Since the FFG parametrization presented here yields the relative enhancement in the retardation factors on functionalized surfaces, i.e., $R(\theta)/R_o$, the results are independent of the absolute magnitude of Kd and can be applied in the most general terms.

It is important to note that saturation will occur on the soil particle surface at some time t, and consequently the retardation will decrease at that time. An alternative way to determine the retardation of a pollutant in soils is to include rate constants for pollutant binding into a chemical transport model. Our SHG vs time traces show that a kinetic analysis is possible not only for the case of the plain silica/water interface (no siloxanes present)[50] but also for the case of the organic-functionalized surfaces. Since the chromate adsorption isotherm measurements are consistent with the notion that K_{ads} increases with coverage, and since K_{ads} is given by k_{ads}/k_{des}, both the adsorption (k_{ads}) and desorption (k_{des}) rate constants may depend on the Cr(VI) surface coverage. If the adsorption process can be described as CrO_4^{2-} (aq) + site $\rightarrow$ Cr(VI) (ads), where "site" represents the adsorption site on the siloxane-functionalized and nonfunctionalized silica/water interfaces, CrO_4^{2-} (aq) represents chromate in the aqueous phase, and Cr(VI) (ads) represents the adsorbed state of Cr(VI), and if the desorption process can be written as the reverse, then the time-dependence of the Cr(VI) surface coverage, θ, can be expressed as

$$\frac{d\theta}{dt} = k_{ads}C_{bulk}(1-\theta) - k_{des}\theta \qquad (7)$$

Since the equilibrium constant for adsorption is given by the FFG model as $K(\theta) = K_{ads} \times \exp(g\theta)$, the adsorption rate constant k_{ads} may be parametrized as $k_{ads} = k_{des}K_{ads}\exp(g\theta)$. Experiments and computer modeling efforts are currently underway to allow for the determination of the adsorption and desorption rate constants. However, it is important to note that the derivation of this FFG-modified kinetic expression for the time-dependence of the Cr(VI) surface coverage assumes equilibrium conditions during chromate adsorption and desorption, which are not necessarily maintained during the experimental conditions. A full analysis of the kinetic experiments will be reported in due course.

V. Conclusions

In conclusion, we have used resonantly enhanced surface second harmonic generation (SHG) to elucidate how surface-bound carboxylic acid and methyl ester functional groups control the interaction of chromate ions with silica/water interfaces at pH 7 and room temperature. The carboxylate functional groups, specifically the carboxylic acid, were chosen because of their high abundance in humic acids and their general importance in biopolymers. The Cr(VI) surface coverage can be measured directly at the interface, in situ, and in real time, and simultaneously with the chromate solution concentrations, which range from 1×10^{-6} to 2×10^{-4} M. By working under neutral pH conditions and in the absence of redox-active metal ions, we can specifically focus on the interaction of Cr(VI) with surface-bound organic functional groups.

We demonstrated that chromate binds to the acid- and ester-functionalized silica/water interfaces in a reversible fashion. Chromate binding studies yielded S-shaped adsorption isotherms for the case of the functionalized silica/water interfaces, which can be modeled using the Frumkin−Fowler−Guggenheim (FFG) model. This model predicts a coverage-dependent binding constant of $K_{ads} \times \exp(g\theta)$, where K_{ads} ranges between $1 \times 10^6 - 2 \times 10^6$ when referenced to the molarity of water in the aqueous solution (55.5 M). Values for the interaction parameter g are 3.2(2), 2.1(2), and 1.3(2) for the carboxylic acid-, the ester- and the nonfunctionalized silica/water interfaces, respectively. These g values are consistent with stabilizing lateral adsorbate−adsorbate interactions and allow us to dissect the overall interaction energies governing chromate binding to the carboxylic acid functional groups into an adsorbate−surface interaction term and an adsorbate−adsorbate interaction term.

The FFG model allows us to parametrize the retardation of chromate in silica-rich soil environments whose particle surfaces contain organic adlayers rich in carboxylic acid and methyl ester groups. This straightforward model predicts that the chromate retardation increases by up to 200% when carboxylic acid functional groups are present at the silica/water interface. Increases by up to 50% are predicted for methyl ester-containing organic adlayers, and the retardation remains effectively near unity for the plain silica/water interface (no siloxanes present). These results show that nonlinear optics methodologies can yield detailed information on the mechanism of toxic metal transport in the environment. These studies will be expanded with the goal of developing a chemical transport model that includes specific adsorption and desorption rate constants. More generally, we can expand our siloxane scaffolds to serve as a versatile chemical platform for generating and studying complex environmentally and biologically important interfaces. This work is an important step in that direction.

Acknowledgment. The authors acknowledge Catherine Schmidt for building the Teflon holder used for depositing the siloxane adlayers on the fused quartz lens. We also thank Spectra Physics and CVI Lasers for donations and the technical support. Financial support for this work was provided by the NSF (CAREER Award CHE-0348873), the ACS-PRF (Grant 38960-G5S), the Northwestern Institute for Environmental Catalysis (CHE-9810378 and DE-FG02-03-ER15457), and the Northwestern Nanoscale Science and Engineering Center (EEC-0118025).

References and Notes

(1) Brown, G. E. *Science* **2001**, *294*, 67−69.
(2) Stumm, W.; Morgan, J. J. *Aquatic Chemistry*, 3rd ed.; Wiley-Interscience: New York, 1996.
(3) Schwarzenbach, R. P.; Gschwend, P. M.; Imboden, D. M. *Environmental Organic Chemistry*, 2nd ed.; John Wiley and Sons: Hoboken, New Jersey, 2003.
(4) Brown, G. E.; Henrich, V. E.; Casey, W. H.; Clark, D. L.; Eggleston, C.; Felmy, A.; Goodman, D. W.; Gratzel, M.; Maciel, G.; McCarthy, M. I.; Nealson, K. H.; Sverjensky, D. A.; Toney, M. F.; Zachara, J. M. *Chem. Rev.* **1999**, *99*, 77−174.
(5) Al-Abadleh, H. A.; Grassian, V. H. *Surf. Sci. Rep.* **2003**, *52*, 63−162.
(6) Evangelou, V. P. *Environmental Soil and Water Chemistry*; John Wiley & Sons: New York, 1998.
(7) Warren, L. A.; Haack, E. A. *Earth-Sci. Rev.* **2001**, *54*, 261−320.
(8) Gustafsson, J. P.; Pechova, P. *Environ. Sci. Technol.* **2003**, *37*, 2767−2774.
(9) Katz, S. A.; Salem, H. *The Biological and Environmental Chemistry of Chromium*; VCH: New York, 1994.
(10) Nriagu, J. O.; Nieboer, E. *Chromium in the Natural and Human Environments*; John Wiley & Sons: New York, 1988.
(11) Goldman, L. R.; Lanphear, B. P. *Science* **1998**, *282*, 1823.
(12) Goyer, R. A.; Klaassen, C. D.; Waalkes, M. P. *Metal Toxicology*; Academic Press: New York, 1995.
(13) Pattison, D. I.; Davies, M. J.; Levina, A.; Dixon, N. E.; Lay, P. A. *Chem. Res. Toxicol.* **2001**, *14*, 500−510.
(14) Arfsten, D. P.; Aylward, L. L.; Karch, N. J. In *Immunotoxicology of Environmental and Occupational Metals*; Zelikoff, J. T., Thomas, P. T., Eds.; Taylor & Francis Inc.: Bristol, PA, 1998.
(15) *National Research Council (US): Committee on Biologic Effects of Atmospheric Pollutants*; National Academy of Sciences: Washington, D.C., 1974; pp 125−145.
(16) Adriano, D. C. *Trace Elements in the Terrestrial Environment*; Springer-Verlag: New York, 1986.
(17) Riley, R. G.; Zachara, J. M.; Wobber, F. J. *Chemical contaminants on DOE lands and selection of contaminant mixtures for subsurface science research*; U.S. Department of Energy: Washington, D.C., 1992.
(18) Spliethoff, H. M.; Hemond, H. F. *Environ. Sci. Technol.* **1996**, *30*, 121−128.
(19) Kaehkoennen, M. A.; Suominen, K. P.; Manninen, P. K.; Salkinoja-Salonen, M. S. *Environ. Sci. Technol.* **1998**, *32*, 1741−1746.
(20) Abu-Saba, K. E.; Flegal, A. R. *Environ. Sci. Technol.* **1997**, *31*, 3455−3460.
(21) van Malderen, H.; Hoornaert, S.; van Grieken, R. *Environ. Sci. Technol.* **1996**, *30*, 489−498.
(22) Wang, W.-X.; Griscom, S. B.; Fisher, N. S. *Environ. Sci. Technol.* **1997**, *31*, 603−611.
(23) Ellis, A. S., Johnson, T. M., Bullen, T. D. *Science* **2002**, *295*, 2060.
(24) Buonicore, A. J. *Cleanup Criteria for Contaminated Soil and Groundwater*; ASTM: West Conshohocken, PA, 1996.
(25) Sena, M. M.; Scarminio, I. S.; Collins, K. E.; Chollines, C. H. *Talanta* **2000**, *53*, 453−461.
(26) Deng, B.; Stone, A. T. *Environ. Sci. Technol.* **1996**, *30*, 463−472.
(27) Swift, R. S. *Soil Sci.* **1999**, *164*, 790−802.
(28) Piccolo, A. *Soil Sci.* **2001**, *166*, 810−829.
(29) Clapp, C. E.; Hayes, M. H. B. *Soil Sci.* **1999**, *164*, 777−789.
(30) Sein L. T., Jr.; Varnum, J. M.; Jansen, S. A. *Environ. Sci. Technol.* **1999**, *33*, 546−552.
(31) Cook, R. L.; Langford, C. H. *Environ. Sci. Technol.* **1998**, *32*, 719−725.
(32) Kinniburgh, D. G.; Milne, C. J.; Benedetti, M. F.; Binheiro, J. P.; Filius, J.; Koopal, L. K.; can de Riemsdijk, W. H. *Environ. Sci. Technol.* **1996**, *30*, 1687−1698.
(33) Wittbrodt, P. R.; Palmer, C. D. *Environ. Sci. Technol.* **1996**, *30*, 2470−2477.
(34) Ephraim, J. H.; Boren, H.; Pettersson, C.; Aresenie, I.; Allard, B. *Environ. Sci. Technol.* **1989**, *23*, 356−362.
(35) Jardine, P. M.; Fendorf, S. E.; Mayes, M. A.; Larsen, I. L.; Brooks, S. C.; Bailey, W. B. *Environ. Sci. Technol.* **1999**, *33*, 2939−2944.
(36) Li, J.; Perdue, E. M.; Gelbaum, L. T. *Environ. Sci. Technol.* **1998**, *32*, 483−487.
(37) Fitch, A.; Du, J. *Environ. Sci. Technol.* **1996**, *30*, 12−15.
(38) Bartschatt, B. M.; Cabaniss, S. E.; Morel, F. M. M. *Environ. Sci. Technol.* **1992**, *26*, 384−394.
(39) Porasso, R. D.; Benegas, J. C.; van den Hoop, M. A. G. T.; OPaoletti, S. *Environ. Sci. Technol.* **2002**, *36*, 3815−3821.
(40) Deng, B.; Stone, A. T. *Environ. Sci. Technol.* **1996**, *30*, 2484−2494.
(41) Buerge, I. J.; Hug, S. J. *Environ. Sci. Technol.* **1998**, *32*, 2092−2099.
(42) Smith, M. B. *Organic Synthesis*; McGraw-Hill: New York, 1994.
(43) Smith, M. B.; March, J. *March's Advanced Organic Chemistry: Reactions, Mechanisms, and Structure*, 5th ed.; John Wiley & Sons: New York, 2001.
(44) Rocek, J.; Ng, C. S. *J. Am. Chem. Soc.* **1974**, *96*, 1522−1529.
(45) Rocek, J.; Ng, C. S. *J. Am. Chem. Soc.* **1974**, *96*, 2840−2846.
(46) Demers, L. M.; Ginder, D. S.; Park, S. J.; Li, Z.; Chung, S. W.; Mirkin, C. A. *Science* **2002**, *296*, 1836−1838.
(47) Cheng, S. S.; Scherson, D. A.; Sukenik, C. N. *Langmuir* **1995**, *11*, 1190−1195.
(48) Voges, A. B.; Al-Abadleh, H. A.; Musorrafiti, M. J.; Bertin, P. A.; Nguyen, S. T.; Geiger, F. M. *J. Phys. Chem. B* **2004**, *108*, 18675−18682.
(49) Konek, C. T.; Musorrafiti, M. J.; Al-Abadleh, H. A.; Bertin, P. A.; Nguyen, S. T.; Geiger, F. M. *J. Am. Chem. Soc.* **2004**, *126*, 11754−11755.
(50) Mifflin, A. L.; Gerth, K. A.; Geiger, F. M. *J. Phys. Chem. A* **2003**, *107*, 9620−9627.
(51) Mifflin, A. L.; Gerth, K. A.; Weiss, B. M.; Geiger, F. M. *J. Phys. Chem. A* **2003**, *107*, 6212−6217.
(52) August, E. E.; Mcknight, D. M.; Hrncir, D. C.; Garhart, K. S. *Environ. Sci. Technol.* **2002**, *36*, 3779−3786.
(53) Tokunaga, T. K.; Wan, J.; Firestone, M. K.; Hazen, T. C.; Schwartz, E.; Sutton, S. R.; Newville, M. *Environ. Sci. Technol.* **2001**, *35*, 3169−3174.

(54) Grossl, P. R.; Eick, M.; Sparks, D. L.; Goldberg, S.; Ainsworth, C. C. *Environ. Sci. Technol.* **1997**, *31*, 32−326.
(55) Weng, C. H.; Huang, C. P.; Allen, H. E.; Leavens, P. B.; Sanders, P. F. *Environ. Sci. Technol.* **1996**, *30*, 371−376.
(56) Fendorf, S.; Eick, M. J.; Grossl, P.; Sparks, D. L. *Environ. Sci. Technol.* **1997**, *31*, 315−320.
(57) Loyaux-Lawniczak, S.; Refait, P.; Ehrhardt, J.-J.; Lecomte, P.; Genin, J.-M. *Environ. Sci. Technol.* **2000**, *34*, 438−443.
(58) Shen, Y. R. *The Principles of Nonlinear Optics*; John Wiley & Sons: New York, 2003.
(59) Eisenthal, K. B. *Chem. Rev.* **1996**, *96*, 1343−1360.
(60) Shen, Y. R. *The Principles of Nonlinear Optics*; John Wiley & Sons: New York, 1984.
(61) Heinz, T. F. *Nonlinear Surface Electromagnetic Phenomena*; Elsevier: Amsterdam, 1991.
(62) Al-Abadleh, H. A.; Voges, A. B.; Bertin, P. A.; Nguyen, S. T.; Geiger, F. M. *J. Am. Chem. Soc.* **2004**, *126*, 11126−11127.
(63) Lagutchev, A. S.; Song, K. J.; Huang, J. Y.; Yang, P. K.; Chuang, T. J. *Chem. Phys.* **1998**, *226*, 337−349.
(64) Masel, R. I. *Principles of Adsorption and Reaction on Solid Surfaces*; John Wiley & Sons: New York, 1996.
(65) Adamson, A. W. *Physical Chemistry of Surfaces*, 5th ed.; John Wiley & Sons: New York, 1990.
(66) Atkins, P. W.; de Paula, J. *Physical Chemistry*, 7th ed.; W. H. Freeman and Company: New York, 2002.
(67) Cantor, C. R.; Schimmel, P. R. *Biophysical Chemistry: The behavior of biological macromolecules (Part III)*; W. H. Freeman and Company: New York, 1980.
(68) Schnitzer, C.; Baldelli, S.; Shultz, M. J. *J. Phys. Chem. B* **2000**, *104*, 585−590.
(69) Schnitzer, C.; Baldelli, S.; Campbell, D. J.; Shultz, M. J. *J. Phys. Chem. A* **1999**, *103*, 6383−6386.
(70) Petersen, P. B.; Saykally, R. J. *Chem. Phys. Lett.* **2004**, *397*, 51−55.
(71) Ghosal, S.; Hemminger, J. C.; Bluhm, H.; Mun, B. S.; Hebenstreit, E. L. D.; Ketteler, G.; Ogletree, D. F.; Requejo, F. G.; M., S. *Science* **2005**, *307*, 563−566.
(72) Raymond, E. A.; Richmond, G. L. *J. Phys. Chem. B* **2004**, *108*, 5051−5059.
(73) Liu, D. F.; Ma, G.; Levering, L. M.; Allen, H. C. *J. Phys. Chem. B* **2004**, *108*, 2252−2260.
(74) Jungwirth, P.; Tobias, D. J. *J. Phys. Chem. A* **2002**, *106*, 379−383.
(75) Ege, S. N. *Organic Chemistry: Structure and Reactivity*, 4th ed.; Houghton Mifflin Co.: Boston, 1999.
(76) Kulkarni, R. M.; Bilehal, D. C.; Nandibewoor, S. T. *Anal. Sci.* **2004**, *20*, 743−747.
(77) Please visit www.epa.gov/radiation/cleanup/partition.htm.
(78) Please visit www.epa.gov/radiation/cleanup/partition.htm, and www.epa.gov/radiation/cleanup/partition.htm.